

## RESEARCH ARTICLE

# Rapid and universal detection of SARS-CoV-2 and influenza A virus using a reusable dual-channel optic fiber immunosensor

Yi Yang<sup>1</sup> | Rongtao Zhao<sup>1</sup>  | Yule Wang<sup>1</sup> | Dan Song<sup>2</sup> | Bo Jiang<sup>3,4</sup> |  
Xudong Guo<sup>1</sup> | Wanying Liu<sup>1</sup> | Feng Long<sup>2</sup> | Hongbin Song<sup>1</sup> |  
Rongzhang Hao<sup>1,3,4</sup> 

<sup>1</sup>Chinese PLA Center for Disease Control and Prevention, Beijing, China

<sup>2</sup>School of Environment and Natural Resources, Renmin University of China, Beijing, China

<sup>3</sup>Department of Toxicology and Sanitary Chemistry, School of Public Health, Capital Medical University, Beijing, China

<sup>4</sup>Beijing Key Laboratory of Environmental Toxicology, Capital Medical University, Beijing, China

## Correspondence

Rongzhang Hao, Department of Toxicology and Sanitary Chemistry, School of Public Health, Capital Medical University, Beijing 100069, China.  
Email: [hao@ccmu.edu.cn](mailto:hao@ccmu.edu.cn)

Hongbin Song, Chinese PLA Center for Disease Control and Prevention, Beijing 100071, China.  
Email: [hongbinsong@263.net](mailto:hongbinsong@263.net)

Feng Long, School of Environment and Natural Resources, Renmin University of China, Beijing 100872, China.  
Email: [longf04@ruc.edu.cn](mailto:longf04@ruc.edu.cn)

## Funding information

National Key Research and Development Program of China, Grant/Award Numbers: 2021YFC2301100, 2019YFC1200604; Capital's Funds for Health Improvement and Research, Grant/Award Number: 2022-2G-4263; National Natural Science Foundation of China, Grant/Award Number: 81871738

## Abstract

Establishment of rapid on-site detection technology capable of concurrently detecting SARS-Cov-2 and influenza A virus is urgent to effectively control the epidemic from these two types of important viruses. Accordingly, we developed a reusable dual-channel optical fiber immunosensor (DOFIS), which utilized the evanescent wave-sensing properties and tandem detection mode of the mobile phase, effectively accelerating the detection process such that it can be completed within 10 min. It could detect the nucleoprotein of multiple influenza A viruses (H1N1, H3N2, and H7N9), as well as the spike proteins of the SARS-CoV-2 Omicron and Delta variants, and could respond to 20 TCID<sub>50</sub>/ml SARS-CoV-2 pseudovirus and 100 TCID<sub>50</sub>/ml influenza A (A/PR/8/H1N1), presenting lower limit of detection and wider linear range than enzyme-linked immunosorbent assay. The detection results on 26 clinical samples for SARS-CoV-2 demonstrated its specificity (100%) and sensitivity (94%), much higher than the sensitivity of commercial colloidal gold test strip (35%). Particularly, DOFIS might be reused more than 80 times, showing not only cost-saving but also potential in real-time monitoring of the pathogenic viruses. Therefore, this newly-developed DOFIS platform is low cost, simple to operate, and has broad spectrum detection capabilities for SARS-CoV-2 mutations and multiple influenza A strains. It may prove suitable for deployment as a rapid on-site screening and surveillance technique for infectious disease.

## KEYWORDS

dual-channel optic fiber immunosensor, influenza A virus, mobile phase detection, SARS-CoV-2

Yi Yang and Rongtao Zhao have equal contribution for this study.

This is an open access article under the terms of the Creative Commons Attribution-NonCommercial-NoDerivs License, which permits use and distribution in any medium, provided the original work is properly cited, the use is non-commercial and no modifications or adaptations are made.

© 2022 The Authors. *Journal of Medical Virology* published by Wiley Periodicals LLC.

## 1 | INTRODUCTION

The high infectivity and strong mutation ability of SARS-CoV-2 may lead to its long-term coexistence with humans.<sup>1</sup> SARS-CoV-2-infected patients typically experience flu-like symptoms, similar to those caused by influenza A virus (FluA). As such, it is hard to distinguish early SARS-CoV-2 infection from FluA infection based solely on symptoms.<sup>2</sup> Since early 2020, the COVID-19 pandemic has prompted countries around the world to strengthen social control measures, which has consequently led to a significant decline in the number of FluA-positive cases. However, with the gradual relaxation of control measures in various countries, the risk of FluA infection has begun to increase again causing significant uncertainty regarding the severity of future outbreaks, as well as the etiologic virus lineage.<sup>3</sup> Moreover, the overlapping seasons of the SARS-CoV-2 pandemic and FluA epidemic may expose a large number of people to an increased risk of simultaneous infection with both viruses. Many case reports show that, compared with a single virus infection, coinfection with SARS-CoV-2 and FluA leads to a rapid development of more serious clinical symptoms.<sup>4</sup> In fact, *in vivo* experiments have shown that FluA infection increases the susceptibility of cells to SARS-CoV-2 infection.<sup>5</sup> Thus, rapid and sensitive differentiation between SARS-CoV-2 and FluA infections has important implications for the management and treatment of patients with influenza-like illness.<sup>6</sup>

Real-time reverse transcription–polymerase chain reaction (rRT-PCR) is presently the gold standard for the diagnosis of SARS-CoV-2 and FluA infections. Several multiplex rRT-PCR test kits, that can simultaneously detect SARS-CoV-2 and FluA, are available.<sup>7,8</sup> These tests primarily require the addition of SARS-CoV-2 and FluA detection primers to an existing multiplex detection system. However, the detection ability of rRT-PCR depends on the copy number and quality of template RNA, which usually requires highly skilled personnel to operate in a sterile environment. Moreover, the entire detection process takes several hours. Simultaneously, the detection of viral RNA cannot directly reflect the infection potential of the virus.<sup>9</sup>

As an important supplementary means for virus detection, immunoassays targeting viral proteins have a higher positive predictive value than rRT-PCR for a virus culture assay (90.0% vs. 73.7%, respectively).<sup>10</sup> Therefore, immune detection targeting viral protein can be used as an important means to assess the transmission risk of SARS-CoV-2 by rRT-PCR-positive individuals. Enzyme-linked immunosorbent assays (ELISAs) and lateral flow immunoassays (LFIAs) are the commonly used immuno-detection methods. ELISA has several operation steps, which impedes rapid detection, and is easily influenced by various factors, such as manual operation differences.<sup>11</sup> Meanwhile, because of its rapid results and simple operation, LFIA is the first choice for a bedside antigen rapid diagnostic test (Ag-RDT); however, its limit of detection (LOD) is high.<sup>12</sup> Therefore, it is urgent to develop more sensitive immuno-assay to improve the efficiency of field screening during the pandemic.

Compared with the above-mentioned detection technologies, biosensors, such as electrochemical biosensors, field-effect sensors, and spectroscopy sensors, offer a number of advantages, including

fast response speed, high sensitivity, convenient use, and low cost.<sup>13,14</sup> The identification interfaces of these biosensors are usually modified with sensitive materials that can specifically bind analytes, such as antigens, antibodies, nucleic acid probes, and aptamers. However, these interfaces are difficult to regenerate after detecting analyte; removing the bound analyte for the next detection not only increases the detection cost, but does not facilitate real-time detection. Moreover, replacement with new identification interfaces often leads to a drift in the baseline detection signal. By contrast, the evanescent field excitation in a mobile phase can make up for a nonreusable detection/identification interface.<sup>15</sup> Such biosensors usually use evanescent waves propagating on the surface of optical waveguides to excite fluorescent-labeled biomolecules (such as antibodies and aptamers) bound on the surface of biosensors. If the refraction angle is greater than the critical angle ( $\theta_c$ ), total reflection occurs at the interface between optical dense medium and optical rare medium when the light propagates along the fiber guide. At each reflection point, there is a finitely attenuated thin electromagnetic field passing through the interface, which penetrates certain distance into medium with a lower refractive index. This field is called the evanescent wave. Because of the limited penetration depth of evanescent waves, which can minimize the interference of free fluorescent molecules, the fluorescent-labeled antibody bound on the biosensor surface and the free fluorescent-labeled antibody in solution can be distinguished without washing steps. According to the linear relationship between the detected fluorescence intensity and the target concentration, quantitative detection can be achieved. In addition, a silicon-based optic fiber can be directly placed in a fluid, thereby limiting the interaction between the optical input/output and the fluid inflow/outflow to the same interface. Thus, the optic fiber has the functions of biological identification and signal transmission, which greatly simplifies the optical structure and makes the detection equipment easy to miniaturize.<sup>16</sup>

In this study, we developed a reusable dual-channel optical fiber immunosensor (DOFIS) for on-site automatic multitype universal detection and identification of SARS-CoV-2 and FluA, which is suitable for dealing with the current complex and changeable situation of epidemic prevention and control, and meaningful for reducing the severe impact of coinfection from the two kinds of important viruses.

## 2 | MATERIALS AND METHODS

### 2.1 | DOFIS design and operation

Based on an indirect immuno-competitive response and tandem detection scheme, a two-channel fiber optic immunoassay DOFIS platform was designed to achieve rapid and sensitive detection of SARS-CoV-2 and FluA. The design scheme is shown in Figure 1. The tandem microfluidic pools of Channel 1 and Channel 2 contained the optic fiber biosensors modified with the FluA nucleoprotein and SARS-CoV-2 spike protein (the details for the preparation of the

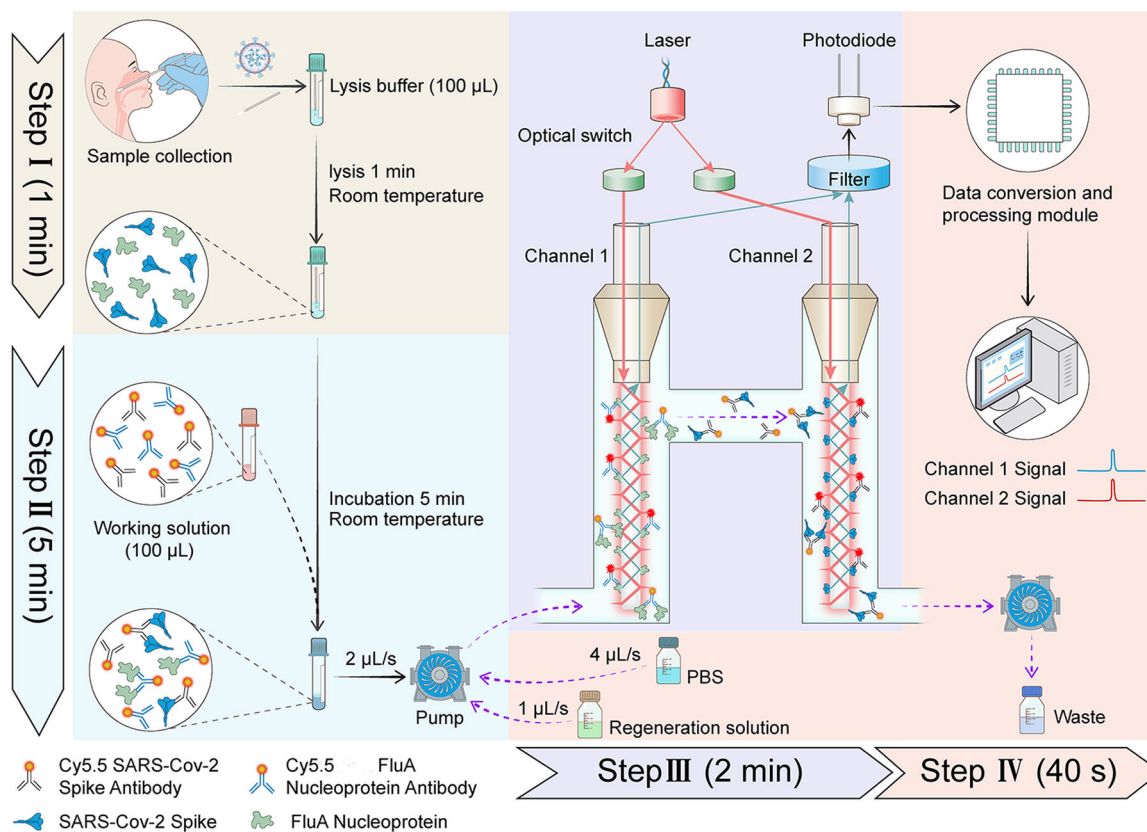


**FIGURE 1** Schematic diagram of the detection of SARS-CoV-2 and FluA using the DOFIS. Different procedures are represented by different background colors. The whole detection procedures from sample in to signal output could be completed within 10 min. DOFIS, dual-channel optical fiber immunosensor; FluA, influenza A virus.

optic fiber biosensors are provided in the Supporting Information), respectively. The laser diode generated the excitation light with a wavelength of 635 nm. The excitation light was propagating through total reflection in Channel 1 and Channel 2, and generated evanescent waves on the surface of the optical fiber biosensor. Due to the limited penetration depth of the evanescent wave (about 100 nm), the evanescent wave just excited the Cy5.5 labeled antibody bound to the antigen modified on the surface of the optical fiber and induced fluorophore excitation, and some fluorescent signals were coupled back to the optical fiber. The multimode optic fiber collected the fluorescence signals, and the photodiode converted the optical signals into electrical signals. The data were collected and processed by the computer. The mobile phase injection module, which consisted of a peristaltic pump, flow channel injection valve, and microfluidic pool, was used to introduce samples, buffer, and the regeneration liquid into the microfluidic pool according to the preset parameters to perform automatic detection.

The analysis cycle included four steps. Step I: throat swabs collected in the clinic were directly immersed in 100 μL of the virus lysis buffer (phosphate-buffered saline [PBS] containing 0.1% NP-40, pH 7.4) and lysed at room temperature for 1 min. Step II: 100 μL of the lysate obtained in Step I was mixed with 100 μL of a working solution (PBS containing the Cy5.5-labeled SARS-CoV-2 spike antibody and Cy5.5-labeled pan-FluA nucleoprotein antibody), and the

mixture was pre-reacted for 5 min. The paratopes of a portion of the Cy5.5-labeled antibody molecules were occupied by antigen proteins. Step III: the pump flow rate was set to 2 μL/s, and PBS (40 s, 80 μL) and the mixed solution (80 s, 160 μL) were sequentially introduced into the microfluidic pool. The Cy5.5-labeled antibody molecules containing free paratopes were captured by the antigen proteins attached to the surface of the optic fiber. The concentration of the target in the sample was quantitatively detected based on difference between the signal values of the sample and the blank control. Step IV: after the detection was completed, the flow rate of the pump was set to 1 μL/s, and a 0.5% SDS (sodium dodecyl sulfate) (pH 1.9) regeneration solution (40 s, 40 μL) was introduced into the microfluidic pool to dissociate the fluorescently labeled antibodies that were captured on the surface of the optic fiber for the fluorescence signal to return to baseline. Finally, the pump flow rate was set to 4 μL/s, and PBS (40 s, 160 μL) was introduced into the microfluidic pool to rinse the optic fiber before detecting next sample.

## 2.2 | Evaluating the performance of the DOFIS with simulated and real clinical samples

To investigate the detection performance of the established DOFIS, clinical simulation samples containing influenza virus strains and

novel coronavirus pseudoviruses were tested and evaluated, and the detection results were compared with LFIA (colloidal gold test strip method), ELISA, or RT-PCR. The used FluA, that is, H1N1 (A/Puerto Rico/8/34/Mount Sinai), was stored in our laboratory. After optimizing the conditions, we focused on testing the detection performance of the DOFIS method for COVID-19 samples. The clinical swab samples related with COVID-19 were stored in the laboratory. Twenty-six swab samples from closely connected with confirmed SARS-CoV-2 cases were examined by RT-PCR laboratory.

## 2.3 | Data analysis

The dose–response curve for the SARS-CoV-2 spike protein or FluA nucleoprotein was fitted with a four-parameter logistic model according to Equation (1):

$$I = (A_1 - A_2)/(1 + ([Ag]/[Ag_0])^p) + A_2, \quad (1)$$

where  $I$  is the normalized signal value from at least three parallel tests;  $A_1$  and  $A_2$  are the upper and lower asymptote to the dose–response curve;  $[Ag]$  is the concentration of target protein, that is, SARS-CoV-2 spike protein or FluA nucleoprotein;  $[Ag_0]$  is the target protein concentration at inflection; and  $p$  is the slope at the inflection point.

Clinical samples were tested by the DOFIS and commercial colloidal gold detection reagents, and their specificity and sensitivity were calculated by Equations (2) and (3), among which TN, FN, TP, and FP were true negative, false negative, true positive, and false positive, respectively.

$$\text{Specificity} = \text{TN}/(\text{TN} + \text{FP}) \times 100\%, \quad (2)$$

$$\text{Sensitivity} = \text{TP}/(\text{FN} + \text{TP}) \times 100\%. \quad (3)$$

T-test was used to analyze the differences between the groups and categorical data were analyzed with Fisher's exact test.  $p < 0.05$  was considered statistically significant.

## 3 | RESULTS AND DISCUSSION

### 3.1 | Establishment of an indirect competitive immunoassay mode

We used the detection mode shown in Supporting Information: Figure S1 to evaluate the modification effect of the optic fiber biosensor and verify that the fluorescent signal came from the specific affinity reaction between the Cy5.5-labeled antibody and the antigen protein that was used to modify the surface of the optic fiber. Figure 2A illustrates the indirect competitive immunodetection mode of the DOFIS for detecting target proteins. The working solution containing a Cy5.5-labeled antibody and the sample containing the detection target were mixed and pre-reacted for 5 min before being

introduced into the microfluidic pool. During the pre-reaction, a portion of the fluorescently labeled antibody paratopes were occupied by the target, thus losing the ability to bind to the antigen on the surface of the optic fiber. Antibody molecules that contained free paratopes were captured by the antigen on the surface of the optic fiber, and Cy5.5 fluorescent molecules were excited by the evanescent wave with a wavelength of 635 nm to generate fluorescent signals. Figure 2B shows a representative real-time fluorescence signal trajectory of the DOFIS detection cycle. At 0–40 s, a PBS was introduced, and the average fluorescence intensity detected by the DOFIS was the detection baseline value  $F_b$ . At 41–120 s, after pre-reaction, the working solution mixed with the sample was introduced into the microfluidic pool. With the antigen on the surface of the optic fiber continuously capturing the Cy5.5-labeled antibody with free paratopes from the mobile phase, the DOFIS-detected fluorescence signal continuously rose to a plateau, reaching a peak at 120 s. At 121–160 s, a 0.5% SDS (pH 1.9) regeneration solution was introduced to dissociate the noncovalently bound antigen and antibody, and the fluorescence signal quickly returned to baseline. Lastly, the residual Cy5.5-labeled antibody was thoroughly washed with PBS for 20 s, after which, the DOFIS was ready for detection of the next sample. The whole detection process, including the pre-reaction, detection, and regeneration, was less than 10 min. The results showed that the real-time signal value of the sample with the target was evidently lower than that of the sample without the target after 60 s, and the difference was stable between 90 and 120 s, which was consistent with the characteristics of the indirect competitive immunoassay mode. Equation (4) was used to calculate the net fluorescence signal values ( $F_{n,b}$  and  $F_{n,s}$ ) of samples without and with targets, respectively.

$$F_n = F_p - F_b. \quad (4)$$

The results in Supporting Information: Figure S1 show that the affinity of Cy5.5–FluA nucleoprotein antibody and Cy5.5–SARS-CoV-2 spike antibody to target proteins was significantly different, suggesting that the detection limit and linear detection range of DOFIS for FluA nucleoprotein and SARS-CoV-2 spike protein may also be different. For the practical application of the DOFIS in the desired dynamic range, the working solution contained the expected median inhibitory concentrations of the FluA nucleoprotein (0.5  $\mu\text{g}/\text{ml}$ ) and SARS-CoV-2 spike protein (0.01  $\mu\text{g}/\text{ml}$ ). The concentration of Cy5.5–FluA nucleoprotein antibody and Cy5.5–SARS-CoV-2 spike antibody were selected according to the following criteria. First, the noncovalently bound antibodies on the surface of optical fibers can be removed by the regeneration solution in no more than 1 min, and short regeneration time could minimize the effect of SDS on the antigen modified on the fiber surface when removing noncovalently bound antibodies; Second, the sensitivity index  $\epsilon$  should be as high as possible, because it would benefit the effective analyte competition in competitive immunoassay, resulting in higher sensitivity. Based on the detection results (Figure 2C,D), when the concentrations of the Cy5.5–FluA nucleoprotein antibody and Cy5.5–SARS-CoV-2 spike antibody in the working solution were 10 and 0.6  $\mu\text{g}/\text{ml}$ , respectively,

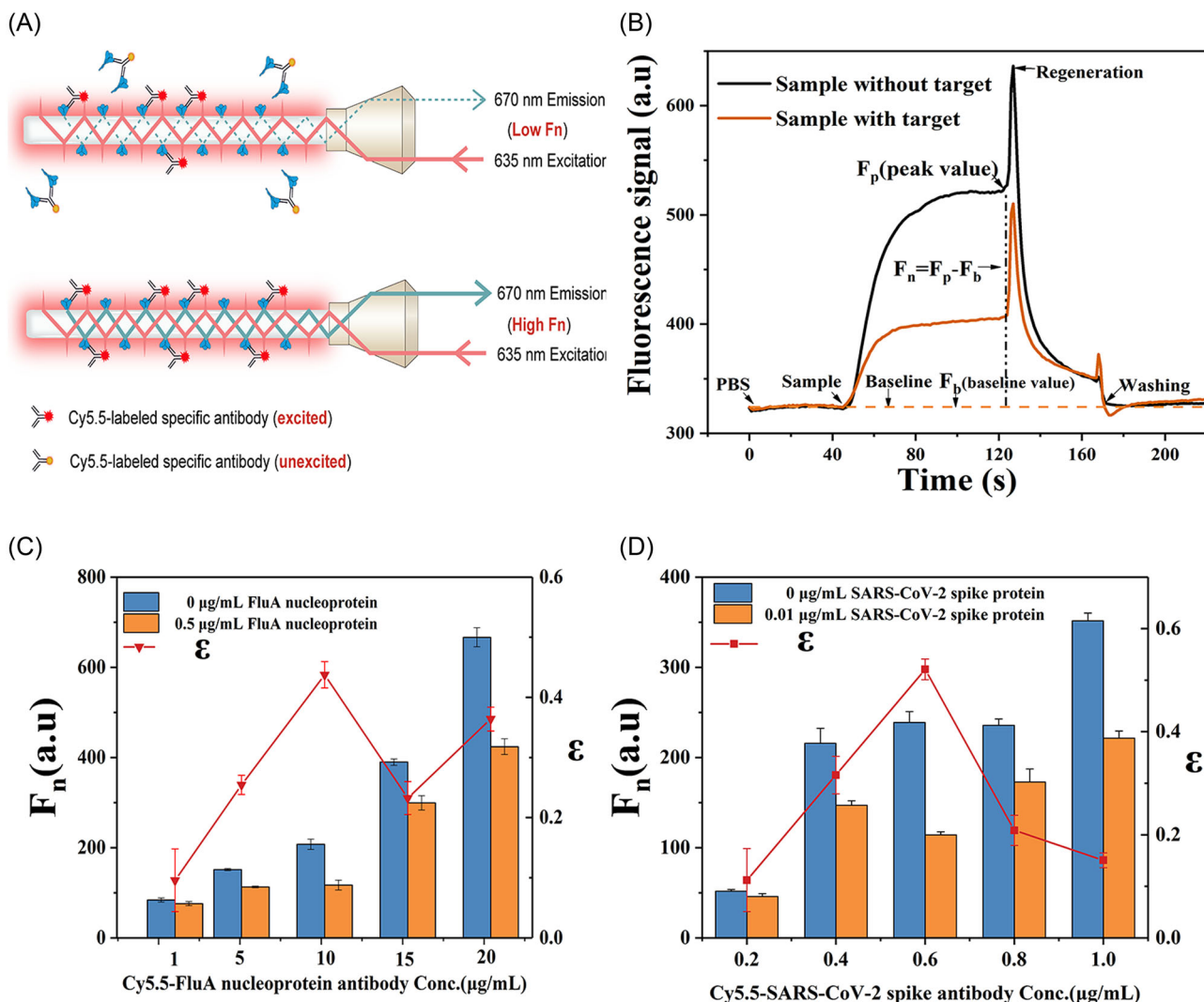


**FIGURE 2** Establishment and optimization of an indirect competitive immunoassay mode. (A) Indirect competitive immunoassay mode of the DOFIS. (B) A typical real-time fluorescence signal track for one period of detection. The working solution was PBS containing 10  $\mu\text{g/ml}$  Cy5.5-FluA nucleoprotein antibody and 0.6  $\mu\text{g/ml}$  Cy5.5-SARS-CoV-2 spike antibody. The sample without a target was a mixture of 100  $\mu\text{l}$  of the working solution and 100  $\mu\text{l}$  of PBS. The sample with a target was a mixture of 100  $\mu\text{l}$  of the working solution and 100  $\mu\text{l}$  of PBS containing 0.01  $\mu\text{g/ml}$  SARS-CoV-2 spike protein. (C, D) Results of the optimization of the (C) Cy5.5-FluA nucleoprotein antibody concentration and (D) Cy5.5-SARS-CoV-2 spike antibody concentration in the working solution. The sensitivity index  $\epsilon = (F_{n,b} - F_{n,s})/F_{n,b}$ . The error bars correspond to the standard deviations of the data points from three repeated experiments ( $n = 3$ ). DOFIS, dual-channel optical fiber immunosensor; FluA, influenza A virus; PBS, phosphate-buffered saline.

the  $\epsilon$  values obtained for Channel 1 and Channel 2 were the highest (0.437 and 0.521, respectively) and the sensing optical fiber can regenerate completely within 40 s. Therefore, the concentrations of 10 and 0.6  $\mu\text{g/ml}$  in the working solution were selected for the Cy5.5-FluA nucleoprotein antibody and Cy5.5-SARS-CoV-2 spike antibody, respectively. In addition, the SARS-CoV-2 and FluA optical fiber biosensors could be reused at least 80 times without a significant decrease in activity (<3%; Supporting Information: Figure S2). Compared with disposable biosensors, the DOFIS showed good reusability, with the advantage of not only avoiding inconsistencies in the detection results due to differences between antibody batches, but also greatly reducing the detection cost.

### 3.2 | Dose-response curves of the FluA nucleoprotein and SARS-CoV-2 spike protein in the indirect competitive immunoassay mode

To obtain the dose-response curves in the indirect competitive immunoassay mode, we mixed different concentrations of the FluA nucleoprotein (0–1500 ng/ml) and SARS-CoV-2 spike protein (0–1000 ng/ml) with an equal volume of a working solution containing 10  $\mu\text{g/ml}$  Cy5.5-FluA nucleoprotein antibody and 0.6  $\mu\text{g/ml}$  Cy5.5-SARS-CoV-2 spike antibody at room temperature for 5 min. During this process, the paratopes of the Cy5.5-labeled antibodies were occupied by the FluA nucleoprotein and SARS-CoV-2 spike

protein, respectively, in different proportions. Subsequently, the mixtures were introduced into the microfluidic pool. Figure 3A,B show the real-time fluorescence signal curves of the DOFIS-detected FluA nucleoprotein and SARS-CoV-2 spike protein, respectively. With the increase in the detection target concentrations, the fluorescence signals detected via Channel 1 and Channel 2 decreased proportionally. To avoid a quenching phenomenon and batch-to-batch differences for fluorescently labeled antibodies, Equation (5) was used to normalize the net fluorescence signal value of each standard concentration:

$$I = F_{n,s}/F_{n,b}. \quad (5)$$

The standard DOFIS-generated curves for the FluA nucleoprotein and SARS-CoV-2 spike protein were typical inverse S-shaped curves in a semilogarithmic coordinate system (Figure 3C,D), which was consistent with the characteristics of dose-response curves in an indirect competitive immunoassay mode. The four-parameter logistic model (Equation 1) was used to fit the standard curves, and the  $R^2$  values were 0.991 and 0.983, respectively. The linear detection ranges of the FluA nucleoprotein and SARS-CoV-2 spike protein by the DOFIS were 225.0–1269.8 and 0.9–77.4 ng/ml, respectively. The standard deviations of the data points in three independent experiments were between 2% and 5% (Figure 3C,D), indicating that the DOFIS could sensitively and stably detect the target concentrations in

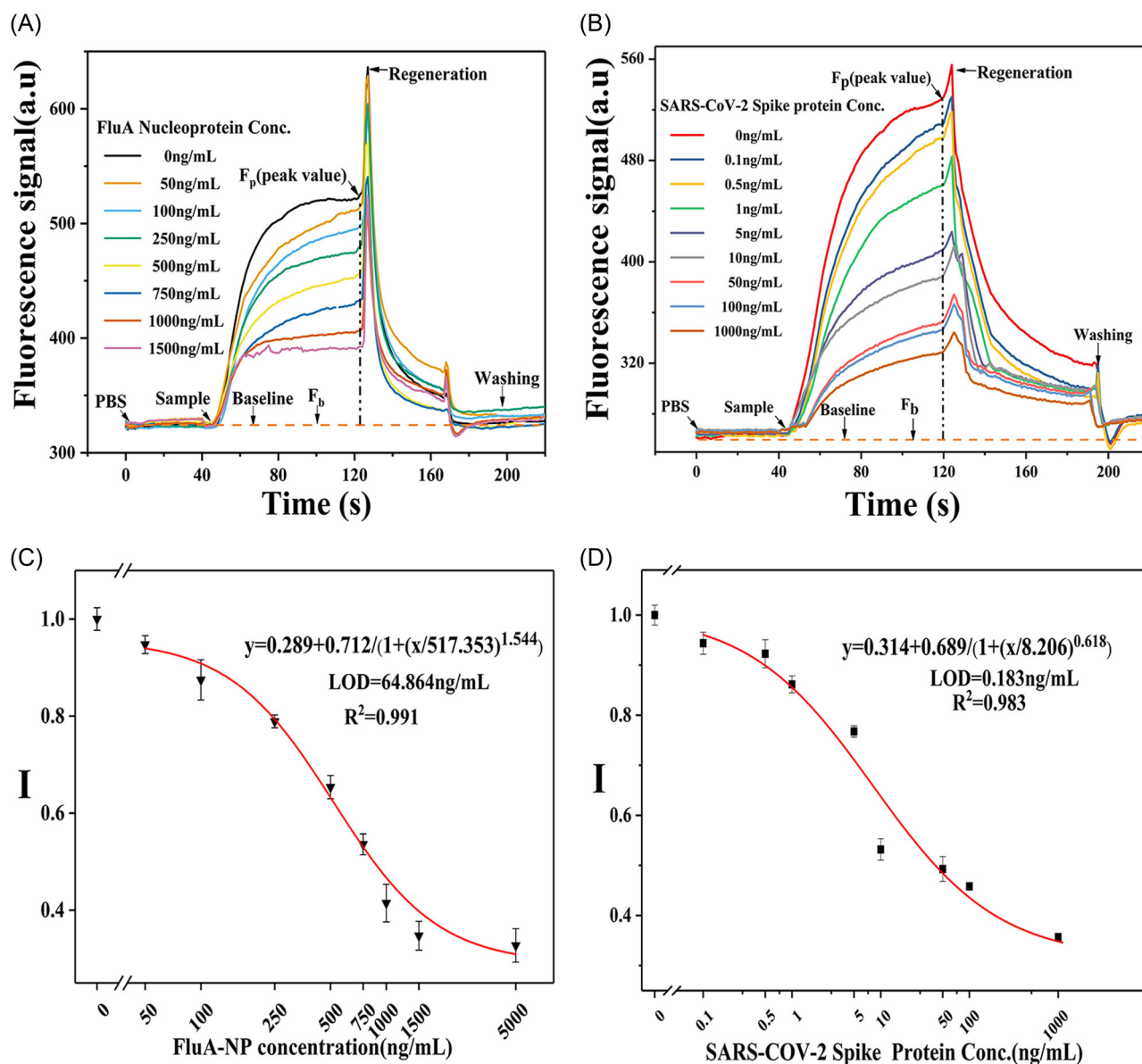


**FIGURE 3** Quantitative detection of the FluA nucleoprotein and SARS-CoV-2 spike protein using the DOFIS. (A, B) Typical real-time fluorescence signal tracks of the (A) FluA nucleoprotein and (B) SARS-CoV-2 spike protein. The working solution was 100  $\mu$ l of PBS containing 10  $\mu$ g/ml Cy5.5-FluA nucleoprotein antibody and 0.6  $\mu$ g/ml Cy5.5-SARS-CoV-2 spike antibody. (C, D) Dose-response curves of the FluA nucleoprotein and SARS-CoV-2 spike protein. The normalized signal value  $I = F_{n,s}/F_{n,b}$ . The error bars correspond to the standard deviations of the data points from three repeated experiments ( $n = 3$ ). DOFIS, dual-channel optical fiber immunosensor; FluA, influenza A virus; PBS, phosphate-buffered saline.

the sample. According to the  $3\sigma$  principle of the normal distribution, recommended by the International Union of Pure and Applied Chemistry, by applying three times the standard deviation of the blank experiment, the limits of detection for the FluA nucleoprotein and SARS-CoV-2 spike protein were determined to be 64.9 and 0.2 ng/ml, respectively. Meanwhile, we investigated the detection performance of ELISAs for the FluA nucleoprotein and SARS-CoV-2 spike protein (Supporting Information: Figure S3). The limits of detection of the DOFIS for the FluA nucleoprotein and SARS-CoV-2 spike protein were lower than those of the ELISA platform (64.9 vs. 167.7 ng/ml and 0.2 vs. 0.5 ng/ml, respectively); moreover, the linear detection ranges were wider for the DOFIS (225.0–1269.8 vs. 253.4–922.4 ng/ml and 0.9–77.4 vs. 2.0–14.6 ng/ml, respectively).

### 3.3 | Verification of the universal detection ability of the DOFIS

To verify the universal detection ability of the DOFIS for many FluA subtypes, we selected the most prevalent FluA subtypes, H1N1, H3N2, and H7N9, as the test samples. Among these, H1N1 and H3N2 cause severe infection in 3–5 million and death of 290 000–650 000 people annually, while, as of February 2020, H7N9 had a global mortality rate as high as 39.2%.<sup>17</sup> In fact, the Center for Disease Control has indicated, through the use of the Influenza Risk Assessment Tool, that among the 12 most novel FluA subtypes, H7N9 has the highest

risk score, which translates to a moderate-to-high potential for causing a pandemic.<sup>18,19</sup>

As shown in Figure 4A, there were no significant differences ( $p > 0.05$ ) among the normalized signal values ( $I$ ) of the DOFIS-detected H1N1 (A/Puerto Rico/8/34/Mount Sinai), H3N2 (A/Hong Kong/2671/2019), and H7N9 (A/Shanghai/2/2013) nucleoproteins at a concentration of 500 ng/ml (0.654, 0.693, and 0.662, respectively); however, these values differed significantly from that of the blank control ( $p < 0.01$ ). These results confirmed a universal detection ability of the DOFIS for the selected FluA subtypes, which is related to conservatism of the detection target protein, that is, nucleoprotein, which exhibits <11% variance among FluA strains.<sup>20</sup>

Beta coronaviruses have caused three zoonotic epidemics, namely, the SARS-CoV epidemic in 2003, the MERS-CoV epidemic in 2012, and the SARS-CoV-2 pandemic in late 2019. Although HCoV-OC43 has low pathogenicity, two new genotypes appeared in 2021, suggesting that routine detection of human respiratory viruses, including the low-pathogenicity coronavirus, should be strengthened to prevent new genotypes from causing regional epidemics. The mutant strains of SARS-CoV-2, B.1.1.529 (Omicron) and B.1.617.2 (Delta), have been the most prevalent variants of concern for COVID-19. The potential ability of the DOFIS to detect SARS-CoV-2 mutants was verified using the spike proteins from SARS-CoV-2 original strain, SARS-CoV-2 Omicron (B.1.1.529), SARS-CoV-2 Delta (B.1.617.2), SARS-CoV, MERS-CoV, and HCoV-OC43 at a concentration of 10 ng/ml. As shown in Figure 4B, the normalized signal values for the SARS-CoV-2 original strain, SARS-CoV-2 Omicron (B.1.1.529), and SARS-CoV-2 Delta (B.1.617.2) spike proteins

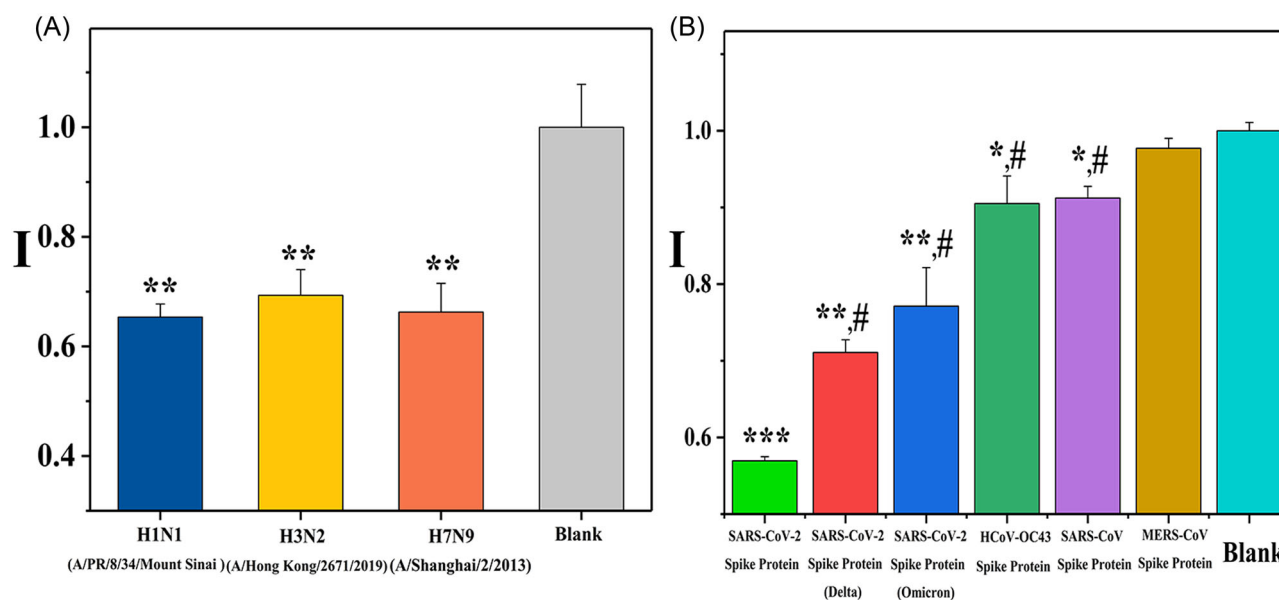


**FIGURE 4** Performance of the DOFIS in universal detection of influenza A viruses (FluA) and coronaviruses. (A) Detection of the nucleoproteins of three FluA subtypes (H1N1, H3N2, and H7N9) at a concentration of 500 ng/ml. (B) Detection of the spike proteins of various coronaviruses [SARS-CoV-2 original strain, SARS-CoV-2 Omicron (B.1.1.529), SARS-CoV-2 Delta (B.1.617.2), SARS-CoV, MERS-CoV, and HCoV-OC43] at a concentration of 10 ng/ml. Each group was tested as a mixture of 100  $\mu$ l of a sample solution (PBS for the Blank control) and 100  $\mu$ l of a working solution. \* $p < 0.05$ , \*\* $p < 0.01$ , and \*\*\* $p < 0.001$  versus the Blank control. # $p < 0.05$  versus the SARS-CoV-2 spike protein. The error bars correspond to the standard deviations of the data points from five repeated experiments ( $n = 5$ ). DOFIS, dual-channel optical fiber immunosensor; PBS, phosphate-buffered saline.

were significantly different from that of the blank control ( $p < 0.05$ ), and the sensitivity was much higher than that against the spike proteins of SARS-CoV, HCoV-OC43, and MERS-CoV. The DOFIS was the most sensitive for the SARS-CoV-2 original strain spike protein, with an  $I$  value as low as 0.569. The lower sensitivity of the DOFIS to the SARS-CoV-2 Omicron (B.1.1.529) and SARS-CoV-2 Delta (B.1.617.2) spike proteins may be related to the mutation sites on the surface of the receptor-binding domain (RBD). There are 15 and 2 mutation sites on the RBD surface of the SARS-CoV-2 Omicron (B.1.1.529) and SARS-CoV-2 Delta (B.1.617.2) spike proteins, respectively, which affect their binding to SARS-CoV-2 spike antibodies.<sup>21,22</sup> In addition, the spike proteins of HCoV-OC43 and SARS-CoV caused an extremely weak signal responses, with  $I$  values of 0.905 and 0.912, respectively. There was no significant difference between the signal caused by MERS-CoV and that in the blank control group. These results may be due to the structural similarity between the spike proteins of these three coronaviruses and SARS-CoV-2 original strain. Superimposition of the spike protein structures of SARS-CoV, HCoV-OC43, and MERS-CoV with that of SARS-CoV-2 original strain showed that the structural similarity values ( $T_m$ ) between the spike proteins of SARS-CoV and HCoV-OC43 and that of SARS-CoV-2 were as high as 0.985 and 0.842, while the value for the MERS-CoV spike protein was only 0.717.<sup>23</sup> Our results show that the DOFIS has the potential to identify a wide spectrum of coronaviruses, however, its sensitivity for SARS-CoV-2 original strain and its variants is much higher than that for other coronavirus strains.

### 3.4 | Testing of simulated virus samples using the DOFIS

We tested the detection capability of the DOFIS with simulated clinical samples, that is, the SARS-CoV-2 spike pseudovirus and FluA strain. The pseudovirus, similar to SARS-CoV-2 particles, expresses

the spike protein on the surface and can be used for quality control of SARS-CoV-2 detection kits.<sup>24</sup> In addition, the FluA strain, H1N1 (A/Puerto Rico/8/34/Mount Sinai), was also chosen as the detection target. Commercial ELISA and colloidal gold technology were used for parallel comparisons with the DOFIS. To mimic the composition of the actual sample, 10% human saliva was added to the virus lysis buffer (PBS containing 0.1% NP-40, pH 7.4). The H1N1 (A/Puerto Rico/8/34/Mount Sinai) strain and SARS-CoV-2 spike pseudovirus were diluted to 20, 100, and 200 TCID<sub>50</sub>/ml with the virus lysis buffer. These six samples and the blank control group were lysed at room temperature for 1 min, then mixed with the working solution, incubated at room temperature for 5 min, and finally introduced into the DOFIS. These samples sequentially flowed through Channel 1 and Channel 2, and the fluorescence signal values were normalized. As shown in Figure 5, Channel 1 sensitively responded to 100 and 200 TCID<sub>50</sub>/ml of H1N1 (A/Puerto Rico/8/34/Mount Sinai), and the normalized signal values ( $I$ ) were significantly different from that in the blank control ( $p < 0.01$ ). It is reported that the LOD of commercial colloidal gold detection reagents for FluA is normally  $1 \times 10^3 - 1 \times 10^5$  TCID<sub>50</sub>/ml.<sup>25</sup> The detection performances of the influenza colloidal gold and ELISA kits were tested for H1N1 (A/Puerto Rico/8/34/Mount Sinai)-simulated clinical samples. The results showed that the colloidal gold detection reagent could not detect H1N1 (A/Puerto Rico/8/34/Mount Sinai) with a titer lower than  $2 \times 10^3$  TCID<sub>50</sub>/ml, and the ELISA only responded to H1N1 with titers higher than 400 TCID<sub>50</sub>/ml (Supporting Information: Figures S4 and S5). Channel 2 sensitively responded to the SARS-CoV-2 spike pseudovirus with a minimum titer of 20 TCID<sub>50</sub>/ml ( $p < 0.01$  vs. the Blank control), while the ELISA did not respond to pseudovirus samples with titers lower than 100 TCID<sub>50</sub>/ml (Supporting Information: Figure S6). The results suggest that the LOD of the DOFIS is much lower than that of the colloidal gold method when detecting FluA (100 vs. 2000 TCID<sub>50</sub>/ml), and also lower than ELISA when

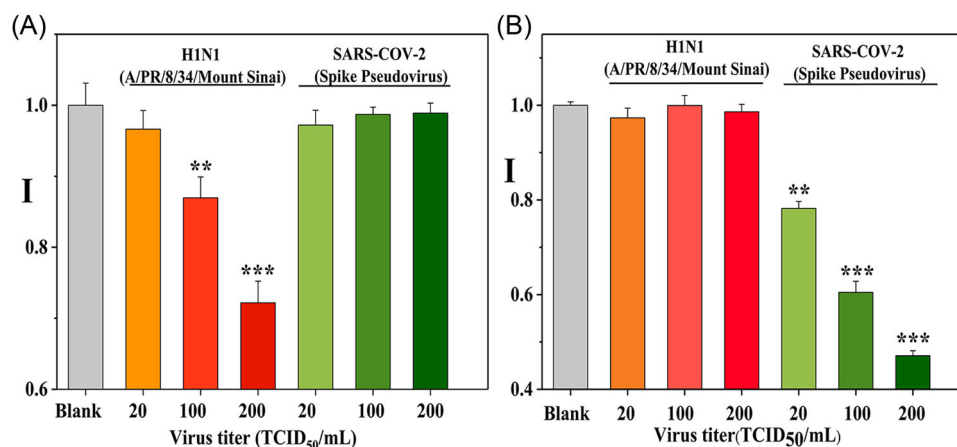


**FIGURE 5** Detection of FluA samples and SARS-CoV-2-simulated samples using the DOFIS. Normalized signal values in (A) Channel 1 and (B) Channel 2 for the detection of FluA samples and SARS-CoV-2-simulated samples. \*\* $p < 0.01$  and \*\*\* $p < 0.001$  versus the Blank control. The error bars correspond to the standard deviations of the data points from five repeated experiments ( $n = 5$ ). DOFIS, dual-channel optical fiber immunosensor; FluA, influenza A virus.

detecting FluA and SARS-CoV-2 pseudovirus (100 vs. 400 TCID<sub>50</sub>/ml and 20 vs. 100 TCID<sub>50</sub>/ml, respectively). In addition, the optic fiber sensors in Channel 1 and Channel 2 showed a good specificity. When the samples containing only the SARS-CoV-2 spike pseudovirus were detected, the fluorescence signal tracks of Channel 1 were similar to that of the blank control group (Supporting Information: Figure S7A), and there was no significant difference between the normalized signal values ( $p > 0.05$  vs. the Blank control; Figure 5A). Similarly, Channel 2 did not respond to samples containing only H1N1 (A/Puerto Rico/8/34/Mount Sinai) ( $p > 0.05$  vs. the Blank control; Figure 5B). These results suggest that the DOFIS is a sensitive and specific assay with a great potential for the detection of FluA and SARS-CoV-2 virus.

### 3.5 | Validation of the DOFIS with COVID-19 samples

As shown in Figure 6A, according to the RT-qPCR test results, there were 9 SARS-CoV-2 negative samples and 17 positive samples with a Ct values of orflab gene between 17.76 and 32.70. The DOFIS and commercial colloidal gold detection reagent gave accurate response to all negative samples. The DOFIS produced significantly different signals toward 16 from 17 positive samples, compared with that toward the blank control group ( $p < 0.05$ ). In contrast, the commercial colloidal gold detection reagent produced only six correct responses from the same positive samples. There was a significant difference

between the detection performance of the DOFIS and commercial colloidal gold detection reagents (Supporting Information: Table S1). According to the receiver operating characteristic curve (ROC curve) shown in Figure 6B, the specificity of the DOFIS and commercial colloidal gold detection reagent were both 100%, but the sensitivity of the DOFIS reached 94%, much higher than the sensitivity of commercial colloidal gold detection reagent (35%). These results suggest that the accuracy of the DOFIS is better than commercial colloidal gold detection reagents. The Ct value or RT-PCR could quantitatively reflect the viral load in the samples. As shown in Figure 6C, the normalized signal value ( $I$ ) of the DOFIS was highly correlated with the Ct value of orflab gene in the samples. The Pearson's correlation coefficient was 0.924,  $p < 0.0001$ , which confirmed that the DOFIS had the ability to quantitatively detect the viral load.

To determine LOD of the DOFIS for clinical samples, the Ct values were converted into viral load by RT-qPCR standard curve (Supporting Information: Figure S8). From the dose response curve of DOFIS for detecting the viral load of clinical samples, the LOD of DOFIS for clinical samples was determined as  $2.3 \times 10^4$  copies/ml (Supporting Information: Figure S9) according to the  $3\sigma$  principle of the normal distribution recommended by the International Union of Pure and Applied Chemistry. However, limited clinical sample number and possible degradation of spike proteins on the surface of virus particles might influence the accuracy of the determination of LOD of DOFIS. Meanwhile, the DOFIS can continuously detect multiple

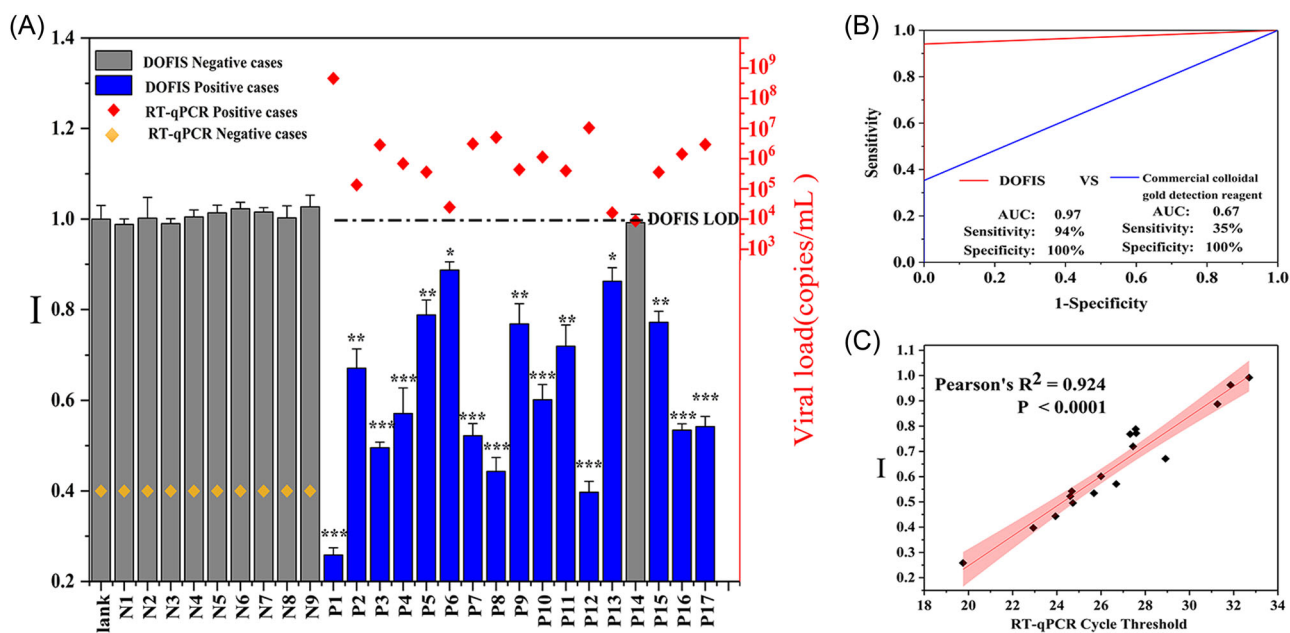


**FIGURE 6** Responses of the DOFIS to COVID-19 clinical samples. (A) Normalized signal values for the detection of throat swab samples from SARS-CoV-2 negative cases and positive cases. viral load of SARS-CoV-2 was shown for all positive cases. (B) ROC curve for detecting clinical samples by the DOFIS and the colloidal gold test strip method. (C) The linear regression with 95% confidence intervals to compare the statistical significance in quantitative response of the DOFIS with that of RT-qPCR. The error bars correspond to the standard deviations of the data points from three repeated experiments ( $n = 3$ ). DOFIS, dual-channel optical fiber immunosensor; ROC, receiver operating characteristic; RT-qPCR, quantitative reverse transcription-polymerase chain reaction.

samples, and multisteps regeneration did not affect the detection performance (Supporting Information: Figure S10). The standard deviation of the signals after regeneration for same samples was less than 5%, as shown in Figure 6A and Supporting Information: Figure S10B.

## 4 | CONCLUSIONS

In this study, we developed a reusable DOFIS for the concurrent detection of SARS-CoV-2 and FluA. Based on the evanescent wave-sensing properties and tandem detection mode of the mobile phase, the DOFIS could universally detect the presence of SARS-CoV-2 (Omicron or Delta variants) or FluA (H1N1, H3N2, and H7N9) within 10 min. The LOD of the DOFIS for the FluA nucleoprotein and SARS-CoV-2 spike protein were as low as 64.9 and 0.2 ng/ml, respectively, better than those of commercial ELISA kits. Moreover, the linear detection ranges of the DOFIS were wider (225.0–1269.8 vs. 253.4–922.4 ng/ml for FluA and 0.9–77.4 vs. 2.0–14.6 ng/ml for SARS-CoV-2, respectively). For virus samples, the DOFIS showed a better detection capability than that of commercial ELISAs and colloidal gold strip method. The DOFIS could specifically detect clinical mock samples of the SARS-CoV-2 pseudovirus with titers of 20 TCID<sub>50</sub>/ml and FluA (PR/8/H1N1) samples with titers of 100 TCID<sub>50</sub>/ml. The specificity and sensitivity of the DOFIS for 26 COVID-19 clinical samples were 100% and 94%, much higher than the sensitivity (35%) of commercial colloidal gold method, and the LOD is as low as  $2.3 \times 10^4$  copies/ml. Moreover, the DOFIS instrument is portable, simple to operate, enabling simultaneous and rapid detection of SARS-CoV-2 and FluA in field conditions. Hence, this platform has significant potential for addressing the likely scenario of concurrent FluA epidemics and constant generation of SARS-CoV-2 mutants, which is significantly meaningful to reduce the disease burden from these two important types of viruses. Particularly, the DOFIS can be reused more than 80 times, without significant decrease in activity (<3%). The reusability of DOFIS not only greatly reduces the detection cost, but also offers a potential platform for further development of real-time infectious disease monitoring.

### AUTHOR CONTRIBUTIONS

**Yi Yang:** Conceptualization, methodology, data curation, writing—original draft, writing—review & editing. **Rongtao Zhao:** Methodology, visualization, writing—original draft, writing—review & editing. **Yule Wang:** Methodology. **Dan Song:** Investigation. **Bo Jiang:** Methodology. **Xudong Guo:** Methodology. **Wanying Liu:** Investigation. **Feng Long:** Conceptualization, investigation, supervision. **Hongbin Song:** Conceptualization, project administration, supervision, writing—review & editing. **Rongzhang Hao:** Conceptualization, methodology, funding acquisition, project administration, supervision, writing—original draft, writing—review & editing.

### ACKNOWLEDGMENTS

This study was supported by the National Key Research and Development Program of China (grant numbers 2021YFC2301100 and 2019YFC1200604), the Capital's Funds for Health Improvement and Research (grant number 2022-2G-4263), and the National Natural Science Foundation of China (grant number 81871738).

### CONFLICT OF INTEREST

The authors declare no conflict of interest.

### DATA AVAILABILITY STATEMENT

The data that supports the findings of this study are available in the supplementary material of this article.

### ORCID

Rongtao Zhao  <http://orcid.org/0000-0002-9845-2405>

Rongzhang Hao  <http://orcid.org/0000-0002-1527-427X>

### REFERENCES

- Cheng ZJ, Qu HQ, Tian L, Duan Z, Hakonarson H. COVID-19: look to the future, learn from the past. *Viruses*. 2020;12(11):1226.
- Rubin R. What happens when COVID-19 collides with flu season? *JAMA*. 2020;324(10):923-925.
- Laurie KL, Rockman S. Which influenza viruses will emerge following the SARS-CoV-2 pandemic? *Influenza Other Respir Viruses*. 2021; 15(5):573-576.
- Liu S, Li W, Jiang S. Disease of influenza virus and SARS-CoV-2 coinfection: flurona or flucovid? *J Med Virol*. 2022;94:4056-4057. doi:10.1002/jmv.27874
- Bai L, Zhao Y, Dong J, et al. Coinfection with influenza A virus enhances SARS-CoV-2 infectivity. *Cell Res*. 2021;31(4):395-403.
- Chotpitayasunondh T, Fischer TK, Heraud JM, et al. Influenza and COVID-19: what does co-existence mean? *Influenza Other Respir Viruses*. 2021;15(3):407-412.
- Au WY, Cheung PPH. Diagnostic performances of common nucleic acid tests for SARS-CoV-2 in hospitals and clinics: a systematic review and meta-analysis. *Lancet Microbe*. 2021;2(12):e704-e714.
- Mostafa HH, Carroll KC, Hicken R, et al. Multicenter evaluation of the Cepheid Xpert Xpress SARS-CoV-2/Flu/RSV test. *J Clin Microbiol*. 2021;59(3):e02955-e02920.
- Sia SF, Yan LM, Chin AWH, et al. Pathogenesis and transmission of SARS-CoV-2 in golden hamsters. *Nature*. 2020;583(7818):834-838.
- Pekosz A, Parvu V, Li M, et al. Antigen-based testing but not real-time polymerase chain reaction correlates with severe acute respiratory syndrome coronavirus 2 viral culture. *Clin Infect Dis*. 2021;73(9):e2861-e2866.
- Michel M, Bouam A, Edouard S, et al. Evaluating ELISA, immunofluorescence, and lateral flow assay for SARS-CoV-2 serologic assays. *Front Microbiol*. 2020;11:597529.
- Cubas-Atienzar AI, Kontogianni K, Edwards T, et al. Limit of detection in different matrices of 19 commercially available rapid antigen tests for the detection of SARS-CoV-2. *Sci Rep*. 2021; 11(1):18313.
- Li J, Lin R, Yang Y, et al. Multichannel immunosensor platform for the rapid detection of SARS-CoV-2 and influenza A(H1N1) virus. *ACS Appl Mater Interfaces*. 2021;13(19):22262-22270.
- Roberts A, Chouhan RS, Shahdeo D, et al. A recent update on advanced molecular diagnostic techniques for COVID-19 pandemic: an overview. *Front Immunol*. 2021;12:732756.

15. Soares MS, Vidal M, Santos NF, et al. Immunosensing based on optical fiber technology: recent advances. *Biosensors (Basel)*. 2021;11(9):305.
16. De Acha N, Socorro-Leránoz AB, Elosúa C, Matías IR. Trends in the design of intensity-based optical fiber biosensors (2010–2020). *Biosensors (Basel)*. 2021;11(6):197.
17. Liu WJ, Xiao H, Dai L, et al. Avian influenza A (H7N9) virus: from low pathogenic to highly pathogenic. *Front Med*. 2021;15(4):507–527.
18. Iuliano AD, Jang Y, Jones J, et al. Increase in human infections with avian influenza A(H7N9) virus during the fifth epidemic—China, October 2016–February 2017. *MMWR Morb Mortal Wkly Rep*. 2017;66(9):254–255.
19. Wang X, Jiang H, Wu P, et al. Epidemiology of avian influenza A H7N9 virus in human beings across five epidemics in mainland China, 2013–17: an epidemiological study of laboratory-confirmed case series. *Lancet Infect Dis*. 2017;17(8):822–832.
20. Cianci C, Gerritz SW, Deminie C, Krystal M. Influenza nucleoprotein: promising target for antiviral chemotherapy. *Antivir Chem Chemother*. 2012;23(3):77–91.
21. Han P, Li L, Liu S, et al. Receptor binding and complex structures of human ACE2 to spike RBD from omicron and delta SARS-CoV-2. *Cell*. 2022;185(4):630–640.
22. Kumar S, Thambiraja TS, Karuppanan K, Subramaniam G. Omicron and Delta variant of SARS-CoV-2: a comparative computational study of spike protein. *J Med Virol*. 2022;94(4):1641–1649.
23. Cueno ME, Imai K. Structural comparison of the SARS CoV 2 spike protein relative to other human-infecting coronaviruses. *Front Med (Lausanne)*. 2021;7:594439.
24. Abrego-Martinez JC, Jafari M, Chergui S, Pavel C, Che D, Sijaj M. Aptamer-based electrochemical biosensor for rapid detection of SARS-CoV-2: nanoscale electrode-aptamer-SARS-CoV-2 imaging by photo-induced force microscopy. *Biosens Bioelectron*. 2022;195:113595.
25. Bai Z, Wei H, Yang X, et al. Rapid enrichment and ultrasensitive detection of influenza A virus in human specimen using magnetic quantum dot nanobeads based test strips. *Sens Actuators B Chem*. 2020;325:128780.

#### SUPPORTING INFORMATION

Additional supporting information can be found online in the Supporting Information section at the end of this article.

**How to cite this article:** Yang Y, Zhao R, Wang Y, et al. Rapid and universal detection of SARS-CoV-2 and influenza A virus using a reusable dual-channel optic fiber immunosensor. *J Med Virol*. 2022;94:5325–5335. doi:10.1002/jmv.28015